# Positron-neutrino correlation in the $0^+ \to 0^+$ decay of $^{32}$Ar

E. G. Adelberger[1], C. Ortiz[2], A. García[2], H.E. Swanson[1], M. Beck[1], O. Tengblad[3], M.J.G. Borge[3], I. Martel[4], H. Bichsel[1] and the ISOLDE collaboration[4]

[1] *Department of Physics, University of Washington, Seattle, Washington 98195-1560*
[2] *Department of Physics, University of Notre Dame, Notre Dame, Indiana 46556*
[3] *Instituto de Estructura de la Materia, CSIC, E-28006 Madrid, Spain*
[4] *EP Division, CERN, Geneva, Switzerland CH-1211*

(February 14, 2014)

The positron-neutrino correlation in the $0^+ \to 0^+$ $\beta$ decay of $^{32}$Ar was measured at ISOLDE by analyzing the effect of lepton recoil on the shape of the narrow proton group following the superallowed decay. Our result is consistent with the Standard Model prediction. For vanishing Fierz interference we find $a = 0.9989 \pm 0.0052 \pm 0.0036$, which yields improved constraints on scalar weak interactions.

23.20.En,13.30.Ce

The $e^+$-$\nu$ correlation in $0^+ \to 0^+$ $\beta$ decay provides a robust signature of possible rare processes where particles other than the usual $W^\pm$ boson are exchanged. In the Standard Model and its left-right symmetric generalizations, $0^+ \to 0^+$ decays produce the $e^+$ and $\nu$ with opposite chiralities. Angular momentum conservation then prevents relativistic leptons from being emitted in *opposite* directions. On the other hand, a scalar interaction, which could arise from exchange of a leptoquark or a Higgs boson [1], will produce the $e^+$ and $\nu$ with identical chiralities so that, in the relativistic limit, the leptons cannot be emitted in *the same* direction. In minimal extensions of the Standard Model, Higgs couplings are too small to affect significantly the $e$-$\nu$ correlation. However, supersymmetric theories with more than one charged Higgs doublet can accommodate sizable scalar couplings [1] that are not ruled out by existing data [2].

This paper reports new constraints on scalar weak interactions based on a precise measurement of the $e$-$\nu$ correlation in the $0^+ \to 0^+$ $\beta^+$ decay of $^{32}$Ar, the only pure Fermi transition whose $e$-$\nu$ correlation has been determined with good precision. The simple spin structure of this decay permits tests for scalar interactions without complications from axial or tensor currents or from recoil-order effects. We consider a $0^+ \to 0^+$ $\beta^+$-decay Hamiltonian [3]

$$H = (\bar{\psi}_n \gamma_\mu \psi_p)(C_V \bar{\psi}_\nu \gamma_\mu \psi_e + C'_V \bar{\psi}_\nu \gamma_\mu \gamma_5 \psi_e) + (\bar{\psi}_n \psi_p)(C_S \bar{\psi}_\nu \psi_e + C'_S \bar{\psi}_\nu \gamma_5 \psi_e) \ , \quad (1)$$

which gives a decay rate

$$\frac{d^3\omega}{dp d\Omega_e d\Omega_\nu} \propto F(Z,p) p^2 E_\nu^2 (1 + a\frac{p}{E}\cos\theta_{e\nu} + b\frac{m}{E}) \times \frac{M_f}{M_i - E + p\cos\theta_{e\nu}} \ , \quad (2)$$

where $E$, $p$ and $m$ are the total energy, momentum and mass of the positron, $E_\nu$ the energy of the neutrino, $M_i$ and $M_f$ are the masses of the parent atom and daughter nucleus, and $F(Z,p)$ the Fermi function. We assume that the Standard Model provides an exact description of the $W^\pm$ exchange process and that $C_V = C'_V$ [4], but make no assumptions on the parity or time-reversal properties of the scalar interaction. Then the $e$-$\nu$ correlation coefficient,

$$a = \frac{2 - |\tilde{C}_S|^2 - |\tilde{C}'_S|^2 + 2Z\alpha m/p \, \mathrm{Im}(\tilde{C}_S + \tilde{C}'_S)}{2 + |\tilde{C}_S|^2 + |\tilde{C}'_S|^2} \ , \quad (3)$$

and the Fierz interference coefficient,

$$b = -2\sqrt{1-(Z\alpha)^2} \, \frac{\mathrm{Re}[\tilde{C}_S + \tilde{C}'_S]}{2 + |\tilde{C}_S|^2 + |\tilde{C}'_S|^2} \ , \quad (4)$$

are functions of $\tilde{C}_S$ and $\tilde{C}'_S$ where

$$\tilde{C}_S = \frac{C_S}{C_V} \quad \text{and} \quad \tilde{C}'_S = \frac{C'_S}{C_V} \ . \quad (5)$$

The $\tilde{C}$'s will be complex if the scalar sector violates time-reversal invariance.

The $e$-$\nu$ correlation must be inferred from the recoil momentum of the daughter nucleus. This traditionally was measured directly, restricting high-precision results to a few favorable cases such as $^6$He [5] and neutron decay [6]. However, if the daughter nucleus is particle unstable, the daughter momentum can be determined from its decay products. This allows one to study energetic light particles rather than slow heavy ions whose atomic and even chemical effects must be considered. Furthermore the transformation from the rest frame of the daughter to the lab amplifies the lepton recoil effects by a factor $2V/v$ where $V$ is the center-of-mass velocity of the light particle and $v$ is the daughter's veleocity due to lepton recoil. Finally, the time scale for particle decay is so short that the delayed particle is emitted before the recoiling daughter can slow down appreciably. Clifford et al. [7] compared the energies of delayed $\alpha$'s detected in coincidence with $\beta$'s emitted toward and away from the $\alpha$, while Schardt and Riisager [8] studied the broadening of narrow delayed proton groups due to lepton recoil. The coincidence technique allows one to measure a *shift* rather than a *spread* which is favorable on statistical grounds and is less sensitive to the response of the charged-particle detector.

On the other hand, the extracted value of the correlation coefficient is very sensitive to the energy and angle of the detected $\beta$ particle. We adopted the singles technique because it seemed difficult to determine the beta's kinematics with sufficient precision.

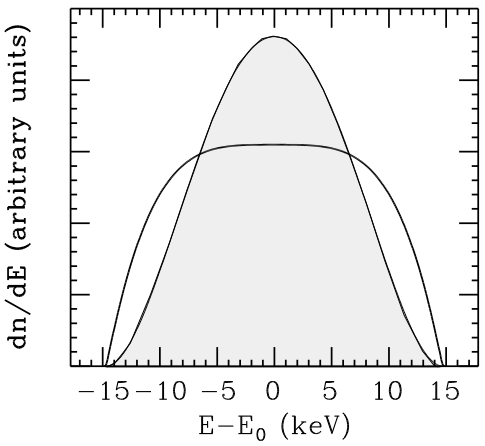


FIG. 1. Intrinsic shapes of the $0^+ \rightarrow 0^+$ delayed proton group for $a = +1,\ b = 0$ (heavy curve) and $a = -1,\ b = 0$ (light curve). The daughter's 20 eV natural width is not visible on this scale.

The kinematics of $^{32}$Ar superallowed decay determine the daughter's velocity distribution and thereby the broadening of the delayed proton peak. The maximum kinetic energy of the recoiling $^{32}$Cl nucleus is

$$T_{\max} = \frac{\Delta^2 - m^2}{2M_i} \tag{6}$$

where $\Delta$ is the difference in atomic masses of the parent and daughter states. The accepted value of $\Delta$ is poorly known because of the $\pm 50$ keV uncertainty in the $^{32}$Ar mass [9]. We use the isospin-multiplet mass equation [10], $M(T_3) = c_0 + c_1 T_3 + c_2 T_3^2$, to obtain an improved value for $\Delta$ from the measured masses of all 5 members of the $A = 32$, $T = 2$ multiplet. These masses, shown in Table I, were obtained from the known ground-state masses and excitation energies [12] of the isobars, except for $^{32}$Cl which we computed from our measured energy of the superallowed delayed-proton peak in $^{32}$Ar decay, $E_{LAB} = 3349.9 \pm 1.2$ keV [13] and the known proton and $^{31}$S masses. The isospin-multiplet mass equation provides an excellent fit to the data and predicts that $\Delta = 3c_2 - c_1 = 6087.3 \pm 2.2$ keV [14], implying $T_{\max} \approx 638$ eV and a maximum daughter velocity of $v = 2.07 \times 10^{-4} c$. The $^{32}$Cl daughter state has a width $\Gamma \approx 20$ eV (see below) so that in one mean life the daughter travels at most $2.1 \times 10^{-2}$Å before emitting the proton. The recoiling $^{32}$Cl therefore emitted the proton while it was still traveling with the full velocity it received from lepton recoil. The intrinsic shape of the delayed proton peak (the shape for a counter with perfect energy resolution) is shown in Fig. 1 for the limiting cases $a = +1,\ b = 0$ and $a = -1,\ b = 0$.

We performed our experiment at ISOLDE. Beams of 60 keV $^{32}$Ar and $^{33}$Ar ions from the General Purpose Separator were focused through a 4 mm diameter collimator and implanted in a 22.7 $\mu$g/cm$^2$ carbon foil inclined at 45° to the beam axis. Protons were detected in a pair of 9 mm × 9 mm PIN diode detectors collimated by 7.72 mm × 7.72 mm apertures located 1.6 cm from the beam axis. We eliminated possible uncertainties from beta summing effects by placing the detection apparatus inside a 3.5 T superconducting solenoid. The magnetic field prevented the betas from reaching the proton detectors (the highest energy betas from the $0^+ \rightarrow 0^+$ decay had $R_c = 0.53$ cm), but had little effect on the protons (the superallowed proton group had $R_c = 7.56$ cm).

The PIN diodes were maintained at −11 C by thermoelectric elements that held the diode temperatures constant to ±0.02 C. The signals were amplified by preamplifiers located immediately outside the vacuum chamber. The preamplifier housings were held at +20 C by thermoelectric devices that held the housing temperatures constant to ±0.01 C. Condensation of vacuum system contaminants on the detectors and stopper foil was minimized by surrounding them with a copper shield cooled by a steady flow of liquid nitrogen. As an added precaution, the detectors were warmed to +27° C once each day to drive off any condensed material. The preamplifier signals were amplified and digitized by modules mounted in temperature-controlled crates and recorded in event-mode by a mini-computer. For each event we recorded the detector energy signals, the absolute time, the delay time after the arrival of a proton pulse, and the temperatures of the detectors, preamps, NIM crate, liquid nitrogen shroud, and the room. Our system gave excellent resolution; the pulser peaks for the two detectors had full-widths at half-maximum of 2.98 and 3.27 keV.

Data were taken over a period of 12 days under several different conditions: with the stopper foil at 45°, 135°, 225° and 315° with respect to the beam axis, and for two different beam tunes. These produced 6 different spectra for each of the 2 counters. We continually alternated between ≈ 2 h long $^{32}$Ar runs and 5-15 min long $^{33}$Ar runs that provided energy calibrations for the $^{32}$Ar data. The $^{32}$Ar and $^{33}$Ar beam intensities on target,

TABLE I. Comparison of the measured mass excesses of the lowest $T = 2$ quintet in $A = 32$ to predictions of the Isobaric Multiplet Mass Equation [$P(\chi^2, \nu) = 0.71$].

| isobar | $T_3$ | $M_{\rm exp}$ (keV)[a] | $M_{\rm IMME}$ (keV) |
|---|---|---|---|
| $^{32}$Si | +2 | $-24080.9 \pm 2.2$ | $-24081.9 \pm 1.4$ |
| $^{32}$P | +1 | $-19232.88 \pm 0.20$[b] | $-19232.9 \pm 0.2$ |
| $^{32}$S | 0 | $-13970.98 \pm 0.41$ [c] | $-13971.1 \pm 0.4$ |
| $^{32}$Cl | −1 | $-8296.9 \pm 1.2$[d] | $-8296.6 \pm 1.1$ |
| $^{32}$Ar | −2 | $-2180 \pm 50$ | $-2209.3 \pm 3.2$ |

[a] unless noted otherwise, ground state masses are from Ref. [9]
[b] $E_x = 5072.44 \pm 0.06$ keV from Ref. [12]
[c] $E_x = 12045.0 \pm 0.4$ keV from Refs. [10,11]
[d] from delayed proton energy [13] and masses of Ref. [9].

averaged over the entire run, were 94 and 3900 ions/s.

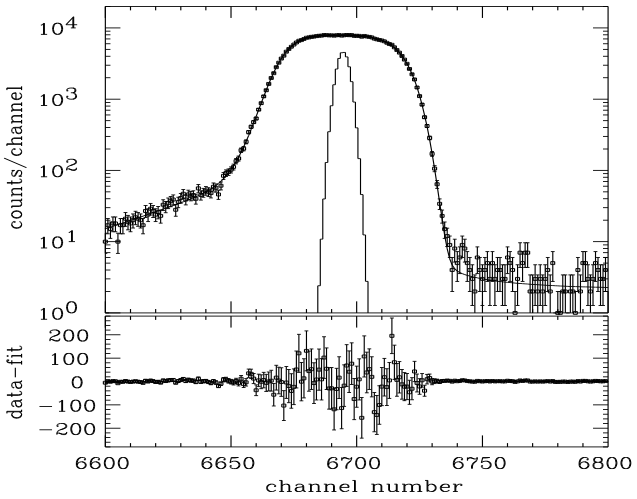


FIG. 2. Fit (upper panel) and residuals (lower panel) of the $0^+ \to 0^+$ delayed proton peak. This spectrum, (the sum of detector 2 data in reflection geometry) contains roughly 1/4 of our data. The energy scale is 0.500 keV/channel. The pulser peak shows the electronic resolution. The Breit-Wigner tail from the 20 eV daughter width is visible on the high-energy side of the peak.

We computed the intrinsic proton shapes using Monte Carlo routines to generate $\beta$-decay events distributed according to Eq. 2 with

$$E_\nu = \frac{(E_{\rm m} - E)}{1 + (p\cos\theta_{e\nu} - E)/M_i} \qquad E_{\rm m} = \Delta - T_{\rm max}\ . \quad (7)$$

The Fermi function for a screened, finite-sized nuclear charge was interpolated from Tables II and III of Ref. [15], and Glück's [16] order-$\alpha$ radiative correction to the energy distribution of recoiling $^{32}$Cl nuclei was applied. A predicted [17] $6.7\times10^{-4}$ electron-capture branch was also included. Protons were ejected isotropically in the $^{32}$Cl frame and deflected by the magnetic field; the mean energy losses of individual protons in the stopper foil and detector dead layer (roughly 1.5 and 1.8 keV, respectively) were computed. The stopper foil thickness was deduced from the energy loss of 3183 keV $^{148}$Gd $\alpha$'s in the foil, while the implantation profile of Ar ions in the foil was computed with TRIM [18]. The detector dead layer thicknesses, $23.4 \pm 0.4$ and $21.6 \pm 0.7$ $\mu$g/cm$^2$, were measured by inserting into the apparatus a jig that allowed the $^{148}$Gd source to be moved along an arc centered on one of the PIN detectors. The dead-layer loss varied as the secant of the angle while the energy loss in the source was essentially constant because the $\alpha$ source was always perpendicular to the line of sight to the detector.

We evaluated the intrinsic proton shape at 961 points on a $\tilde{C}_S$-$\tilde{C}'_S$ grid. The intrinsic shapes plus a small, flat background were convoluted with a proton detector response function consisting of 2 low-energy exponential tails folded with a Gaussian. This functional form gave a good parameterization of a "first principles" calculation of the response function that included the effects of pulser resolution, the Fano factor, electronic and nuclear straggling in the stopper foil and detector dead layer, escape of Si X-rays, and energy loss to phonon excitations of the detector. We fitted our 6 pairs of delayed-proton spectra by varying the response function parameters (Gaussian width, tail lengths and fractional areas) to minimize $\chi^2$ for each $\tilde{C}_S$, $\tilde{C}'_S$ point. Figure 2 displays the quality of the fits. Figure 3 shows that the extracted lineshape agreed well with the "first-principles" calculation. Fits were made for a series of values of $\Gamma$, the natural width of the daughter. There was essentially no correlation between $\Gamma$ and $\tilde{C}_S$ and $\tilde{C}'_S$, and we found $\Gamma = 20 \pm 10$ eV.

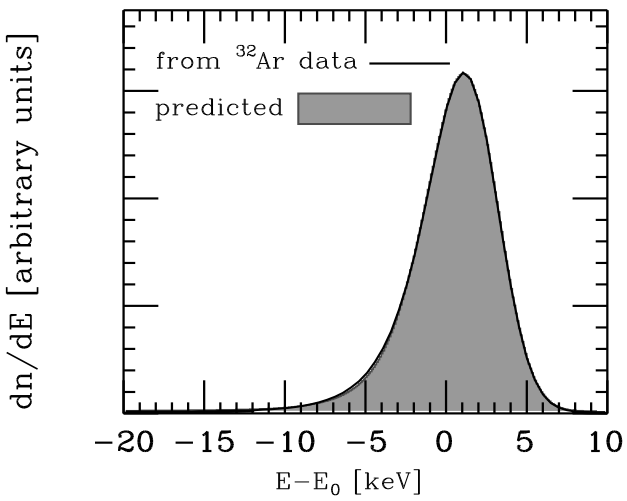


FIG. 3. Comparison of the detector response function extracted from the data in Fig. 2 to the "first-principles" calculation described in the text.

Figure 4 shows constraints on $\tilde{C}_S$ and $\tilde{C}'_S$ from this work and from Refs. [19–23]. The annular shapes of our constraints arise from the Fierz interference term in Eq. 2. Our $\tilde{C}_S$-$\tilde{C}'_S$ constraints may be parameterized as

$$\tilde{a} \equiv a/(1 + 0.1913b)$$
$$= 0.9989 \pm 0.0052(\text{stat.}) \pm 0.0036(\text{syst.})\ 68\%\ \text{c.l.} \quad (8)$$

where $a$ and $b$ are given in Eqs. 3, 4 with $\langle m/p \rangle = 0.21$. Note that $\tilde{a}$, unlike $a$, does not have an upper bound of $+1$, so the range spanned by our experimental $2\sigma$ error band lies entirely within the physical region.

The systematic error included in Eq. 8 and Fig. 4 was evaluated by combining in quadrature the following effects. We found the dependence of $\tilde{a}$ on the exact values of $\Delta$ and $Q_p$, $\partial\tilde{a}/\partial\Delta = -1.2 \times 10^{-3}$ keV$^{-1}$ and $\partial\tilde{a}/\partial Q_p = -0.9 \times 10^{-3}$ keV$^{-1}$, by repeating the entire analysis with $\Delta$ and $Q_p$ changed by $\pm10$ keV. The uncertainties, $\delta\Delta = \pm2.2$ keV and $\delta Q_p = \pm1.2$ keV, gave a *kinematic* systematic error $\delta\tilde{a} = \pm0.0032$. [24] We

checked the dependence of $\tilde{a}$ on the *fitting regions* of the proton spectra; a 28% variation in the width of the region changed $\tilde{a}$ by less than $\pm 0.00055$. We examined the dependence of our results on the form of the detector response function by reanalysing the data with a single-tail response function; by reanalyzing the data assuming that a weak Gamow-Teller peak lay under the tail of the $^{32}$Ar superallowed peak; and by simultaneously fitting the $^{33}$Ar and $^{32}$Ar superallowed peaks using a common response function. From these tests we inferred a *line-shape* systematic error of $\delta\tilde{a} = \pm 0.0016$.

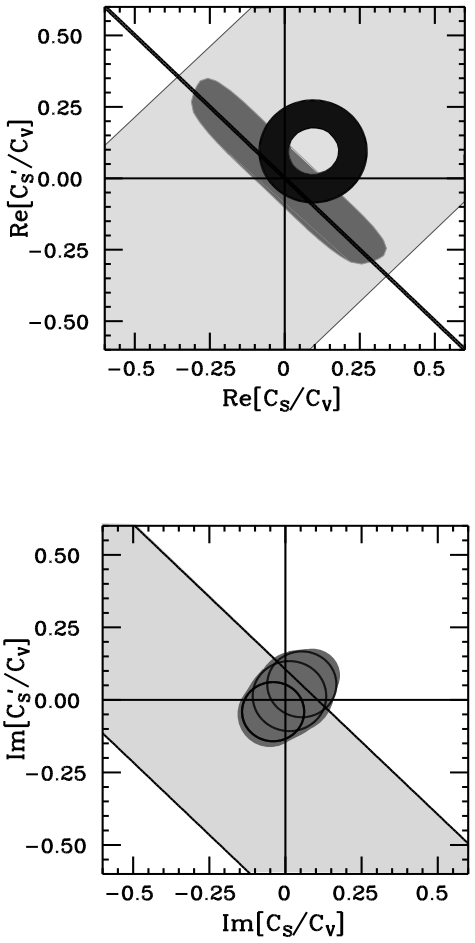


FIG. 4. 95% conf. limits on $\tilde{C}_S$ and $\tilde{C}'_S$. Upper panel: time-reversal-even couplings. The annulus is from this work. The narrow diagonal band is from $b(0^+ \to 0^+)$ [19]. The broad diagonal band shows constraints from $A$, $B$, $a$, and $t_{1/2}$ in $n$ decay [20]; the sausage-shaped area includes, in addition, constraints from $G(^{14}\mathrm{O})$ and $G(^{10}\mathrm{C})$ [21], $b(^{22}\mathrm{Na})$ [22] and $a(^{6}\mathrm{He})$ [5]. Lower panel: time-reversal-odd couplings. The circles are from this work and correspond to $\tilde{C}_S$ and $\tilde{C}'_S$ phases of $\pm 90°$, $+45°$ and $-45°$. The shaded oval shows the constraint with no assumptions about this phase. The diagonal band is from $R(^{19}\mathrm{Ne})$ [23].

For scalar interactions with $\tilde{C}_S = -\tilde{C}'_S$ so that $b = 0$, we obtain a $1\sigma$ limit $|\tilde{C}_S|^2 \leq 3.6 \times 10^{-3}$. The corresponding limit on the mass of scalar particles with gauge coupling strength is $M_S = |\tilde{C}_S|^{-1/2} M_W \geq 4.1 M_W$.

We thank T. Van Wechel and H. Simons for help constructing the apparatus, J.J. Kolata and F. Bechetti for lending us the superconducting magnet, D. Forkel-Wirth for help setting up our apparatus at CERN, and B. Jennings and I. Bigi for useful remarks. This work was supported in part by the DOE (at the University of Washington) and by the NSF and the Warren Foundation (at the University of Notre Dame).

[1] P. Herzeg, in *Precision Tests of the Standard Electroweak Model*, World Scientific, P. Langacker ed., 768 (1995).
[2] A.I. Boothroyd, J. Markey, and P. Vogel, Phys. Rev. C, **29** 603 (1984).
[3] J.D. Jackson, S.B. Treiman, and H.W. Wyld Jr., Nucl. Phys. **4**, 206 (1957).
[4] We neglect possible small leptoquark-exchange contributions to $C_V$ and $C'_V$.
[5] C.H. Johnson, F. Pleasanton and T.A. Carlson, Phys. Rev. **132**, 1149 (1963).
[6] C. Stratova *et al.*, Phys. Rev. D. **18**, 3970 (1978).
[7] E.T.H. Clifford *et al.*, Nucl. Phys. **A493**, 293 (1989).
[8] D. Schardt and K. Riisager, Z. Physik A **345**, 265 (1993).
[9] G. Audi and A.H. Wapstra, Nucl. Phys. A **595**, 409 (1995).
[10] M.S. Antony *et al.*, At. Data Nucl. Data Tables **33**, 447 (1985).
[11] G. Walter, private communication (1998).
[12] P.M. Endt, Nucl. Phys. **A521**, 1 (1990).
[13] The error is dominated by the uncertainties in the energies of the $^{33}$Cl daughter states fed in $^{33}$Ar decay.
[14] There is no evidence for any violation of the IMME, $P(\chi^2, \nu)$ drops to 0.52 when a $c_3 T_3^3$ term is added.
[15] H. Behrens and J. Jänecke, Landolt-Börnstein, New Series, Group I, Vol. **4**, *Numerical Tables for Beta-Decay and Electron Capture*, ed. H. Schopper, Springer-Verlag, Berlin (1969).
[16] F. Glück, Nucl. Phys. **A628**, 493 (1998).
[17] N.B. Gove and M.J. Martin, Nucl. Data. At. Data Tables **10**, 206 (1971).
[18] Written and distributed by J.F. Ziegler.
[19] W.E. Ormand, B.A. Brown and B.R. Holstein, Phys. Rev. C **40**, 2914 (1989).
[20] Particle Data Group, Eur. Phys. J. **C 3**, 622 (1998).
[21] A.S. Carnoy *et al.*, Phys. Rev. C **43**, 2825 (1991).
[22] H. Wenninger, J. Stiewe, and H. Leutz, Nucl. Phys. **A 109**, 561 (1968).
[23] M.B. Schneider *et al.*, Phys. Rev. Lett. **51**, 1239 (1983).
[24] We account for the correlation between $\Delta$ and $Q_p$.